Molecular Therapy
Methods & Clinical Development
Original Article

Visceral adipose tissue-directed FGF21 gene therapy improves metabolic and immune health in BTBR mice

Nicholas J. Queen,[1,2] Rhiannon Bates,[1,2] Wei Huang,[1,2] Run Xiao,[1,2] Bhavya Appana,[1,2] and Lei Cao[1,2]

[1]Department of Cancer Biology & Genetics, College of Medicine, The Ohio State University, Columbus, OH 43210, USA; [2]The Ohio State University Comprehensive Cancer Center, Columbus, OH 43210, USA

Fibroblast growth factor 21 (FGF21) is a peptide hormone that serves as a potent effector of energy homeostasis. Increasingly, FGF21 is viewed as a promising therapeutic agent for type 2 diabetes, fatty liver disease, and other metabolic complications. Exogenous administration of native FGF21 peptide has proved difficult due to unfavorable pharmacokinetic properties. Here, we utilized an engineered serotype adeno-associated viral (AAV) vector coupled with a dual-cassette design to selectively overexpress FGF21 in visceral adipose tissue of insulin-resistant BTBR T+Itpr3tf/J (BTBR) mice. Under high-fat diet conditions, a single, low-dose intraperitoneal injection of AAV-FGF21 resulted in sustained benefits, including improved insulin sensitivity, glycemic processing, and systemic metabolic function and reduced whole-body adiposity, hepatic steatosis, inflammatory cytokines, and adipose tissue macrophage inflammation. Our study highlights the potential of adipose tissue as a FGF21 gene-therapy target and the promise of minimally invasive AAV vectors as therapeutic agents for metabolic diseases.

INTRODUCTION

Fibroblast growth factor 21 (FGF21) is a peptide hormone that acts on various tissues to maintain energy homeostasis. While FGF21 production predominately occurs in the liver, adipocytes are the main target of FGF21 action.[1–5] In white adipose tissue (WAT), FGF21 stimulates glucose uptake in an insulin-independent manner,[6] modulates lipolysis,[3] regulates mitochondrial activity,[7] and regulates adaptive thermogenesis.[8] Furthermore, the antidiabetic actions of FGF21—resulting in improvements in obesity-induced hyperglycemia, hypertriglyceridemia, and peripheral insulin resistance—are thought to occur primarily within WAT.[1,2]

The therapeutic potential of FGF21 is well recognized by the metabolism, pharmaceutical, and gene therapy communities. Increasingly, FGF21 is viewed as a potential therapeutic agent for type 2 diabetes (T2D), fatty liver disease, and other metabolic complications.[9] Exogenous administration of recombinant FGF21 protein to *ob/ob*, *db/db*, and high-fat diet (HFD) mice reduces adiposity, lowers blood glucose and triglycerides, and improves insulin sensitivity.[6,10,11] Despite early successes, use of native FGF21 peptide was found to be unfavorable due to its short half-life and biophysical deficiencies.[12] While the development of FGF21 analogs and mimetics is ongoing and provides promise, some limitations exist. The use of FGF21 protein analogs or mimetics may require repeated administrations for maintained clinical benefit, which raises concerns about immunological reactions associated with exogenous protein administration, patient comfort, and treatment non-compliance.[13–15]

Recent work in the field has investigated the use of adeno-associated viral (AAV) vectors for FGF21 gene therapy to treat obesity and insulin resistance.[16,17] AAV vectors serve as one solution for the troubles of long-term therapeutic protein administration, as they require a single administration for long-term transgene production. AAV vectors are predominately non-integrative, and their genomes persist as episomes in non-dividing cells.[18] Variations in AAV capsids yield tissue tropism, making AAVs adaptable for various therapeutic-, tissue- and cell-specific applications.[19]

WAT is a dynamic endocrine and secretory organ, serving as much more than a mere vessel for energy storage.[20] Visceral adipose tissue (VAT) is a subtype of WAT that surrounds inner organs in the abdominal cavity and is thought to contribute to local/systemic inflammation and metabolic function.[21,22] Mature adipocytes in WAT depots are terminally differentiated,[23] making them an attractive target for primarily non-integrative gene expression vectors such as AAVs. Recently, we characterized a novel engineered hybrid serotype, Rec2, which achieves superior transduction of adipose tissue when compared to naturally occurring AAV serotypes.[24] We and others have applied Rec2 serotype vectors to manipulate adipose depots of interest in various mouse models.[24–32] Furthermore, we recently designed a dual-cassette vector to transduce VAT in a highly selective manner, while severely restricting off-target transduction of liver during non-invasive intraperitoneal (i.p.) administration.[25,31,32] Here, we combine these unique delivery systems to investigate the

Received 24 September 2020; accepted 21 December 2020;
https://doi.org/10.1016/j.omtm.2020.12.011.

Correspondence: Lei Cao, PhD, Department of Cancer Biology & Genetics, College of Medicine, The Ohio State University, 460 W 12th Ave, Columbus, OH 43210, USA.
E-mail: lei.cao@osumc.edu

potential for WAT-targeted FGF21 gene therapy in obese, insulin-resistant BTBR T+Itpr3tf/J (BTBR) mice.[33]

RESULTS

To investigate the potential of WAT-directed FGF21 gene therapy to improve metabolic dysregulation, we utilized adipose-targeting recombinant AAV (rAAV)-Rec2 vector containing two expression cassettes, one driving the transgene expression by a constitutive promoter, while the second cassette uses a liver-specific promoter to express a microRNA targeting the woodchuck post-transcriptional regulatory element (WPRE) sequence existing in the first cassette (Figure 1A). i.p. injection of the Rec2 dual-cassette vector achieves selective transduction of visceral adipose depots while severely restricting off-target transgene expression in the liver.[25,31,32] This VAT-directed FGF21 gene therapy was applied to insulin-resistant BTBR mice under normal chow diet (NCD) and diet-induced obesity (DIO) conditions.

Intraperitoneal administration of Rec2-FGF21 sustains FGF21 overexpression in VAT and alters hypothalamic gene expression under NCD conditions.

NCD-fed mice were injected i.p. with 2.0×10^{10} vg of either Rec2-FGF21 or a control vector containing no transgene, Rec2-Empty (Figure 1A). Mice were subjected to various metabolic tests over a 21-week period (Figure 1B). No differences in body weight (Figure 1C) or food intake (Figure 1D) were observed over 21 weeks. An *in vivo* echoMRI at 4, 7, and 21 weeks post-injection revealed no significant differences in body fat (Figures 1E, S1A, and S1B) or lean mass percentage (Figures 1F, S1C, and S1D). At 5 weeks post-AAV injection, mice were subjected to a glucose tolerance test (GTT) to assess systemic glycemic processing; no significant differences were observed (Figures 1G and 1H). At 11 weeks post-AAV injection, an open-field (OF) test was performed; no differences in anxiety-like behaviors and locomotion were observed (Figures S1E–S1G). From 12 to 14 weeks post-AAV injection, indirect calorimetry was performed. No significant differences between Rec2-FGF21 and Rec2-Empty groups were observed across various metrics, including VO_2, VCO_2, respiratory exchange ratio (RER), and ambulation (Figures S2A–S2H). At 20 weeks post-AAV injection, an insulin tolerance test (ITT) revealed no significant differences in non-fasting glucose levels or insulin sensitivity between the two groups (Figures 1I and 1J). At 21 weeks post-injection, tissues and serum were collected. Rec2-FGF21 and Rec2-Empty mice displayed no significant differences in relative tissue mass of brown adipose tissue (BAT), inguinal WAT (iWAT), gonadal WAT (gWAT), retroperitoneal WAT (rWAT), liver, or pancreas (Figure 1K).

Rec2-FGF21-treated mice exhibited an approximately 10-fold elevation of serum FGF21 (Figure 1L). No change in serum leptin (Figure 1M) or chemokine (C-C motif) ligand 2 (CCL2, also known as MCP-1) was observed (Figure 1N). Consistent with serum data, a robust 100-fold upregulation of *Fgf21* expression was observed in the gWAT (Figure 1O). Together, these data indicate that Rec2-FGF21 sufficiently upregulated local and systemic FGF21 levels over the duration of the 21-week study, although no functional changes in systemic metabolism were observed under NCD conditions.

Given that FGF21 acts centrally,[34–36] we additionally profiled hypothalamic tissue to assess gene-therapy-induced alterations in neuroendocrine and inflammation markers (Figure S3). FGF21 acts on a receptor complex consisting of the ubiquitously expressed FGF receptor 1 (encoded by *Fgfr1*) and a co-receptor β-klotho (encoded by *Klb*) that is restricted to specific metabolic tissues including adipose tissue, liver, and particular areas of brain.[37,38] No changes in *Fgfr1* and *Klb* were observed. The Rec2-FGF21-treated group exhibited a trend of upregulation of *Crh* (encoding corticotropin-releasing hormone), consistent with peripheral upregulation of FGF21.[34] A trend of downregulation of *Insr* (encoding insulin receptor) was observed in the Rec2-FGF21-treated group. No changes in other neuropeptides or receptors involved in energy balance including *Obrb* (encoding leptin receptor), *Npy* (encoding neuropeptide Y), *Pomc* (encoding proopiomelanocortin), or *TrkB-FL* (encoding full-length tropomyosin receptor kinase B) were observed. Interestingly, a bevy of inflammatory cytokines and immune modulatory genes—including *Ccl2*, *Il1b* (encoding interleukin-1β), *Ikbkb* (encoding inhibitor of nuclear factor kappa-B kinase subunit beta), *Tnfa* (encoding tumor necrosis factor alpha), *Il33* (encoding interleukin-33), and *H2Ab1* (encoding histocompatibility 2, class II antigen A, beta)—were collectively downregulated in the hypothalamus of the Rec2-FGF21 group.

VAT-directed overexpression of FGF21 improves systemic metabolism in DIO mice

Following 4 weeks of HFD feeding, a separate DIO cohort of mice was injected i.p. with 2.0×10^{10} vg of either Rec2-FGF21 or Rec2-Empty. Mice were subjected to various metabolic tests over a 16-week period (Figure 2A). No differences in absolute body weight were observed over the course of the experiment (Figure 2B). While Rec2-Empty mice continued to gain weight, we observed a moderation in DIO-induced weight gain in Rec2-FGF21-injected mice (Figure 2C). In tandem with these observations, Rec2-FGF21 mice exhibited increased relative food consumption calibrated to body weight, suggesting an increase in energy expenditure (Figure 2D). An *in vivo* echoMRI revealed Rec2-FGF21 mice to have a reduced body fat percentage (Figures 2E and S4A) and increased lean mass percentage (Figures 2F and S4B) when compared to Rec2-Empty controls. At 8 weeks post-AAV injection, mice were subjected to an ITT. Rec2-FGF21 mice showed significantly lower non-fasting blood glucose levels (at t = 0) and improved overall response to the ITT (Figures 2G and 2H), indicative of alleviation of insulin resistance in the obese BTBR mouse model. At 10 weeks post-AAV-injection, an OF test was performed; no differences in anxiety-like behaviors and locomotion were observed (Figures S4C–S4E). At 10 weeks post-AAV-injection, a GTT was performed. Rec2-FGF21 mice cleared an i.p. glucose bolus in a more efficient manner, indicating an improvement in glycemic processing following FGF21 gene therapy (Figures 2I and 2J).

From 11 to 14 weeks post-AAV-injection, mice were subjected to indirect calorimetry. Rec2-FGF21 mice exhibited an increased oxygen

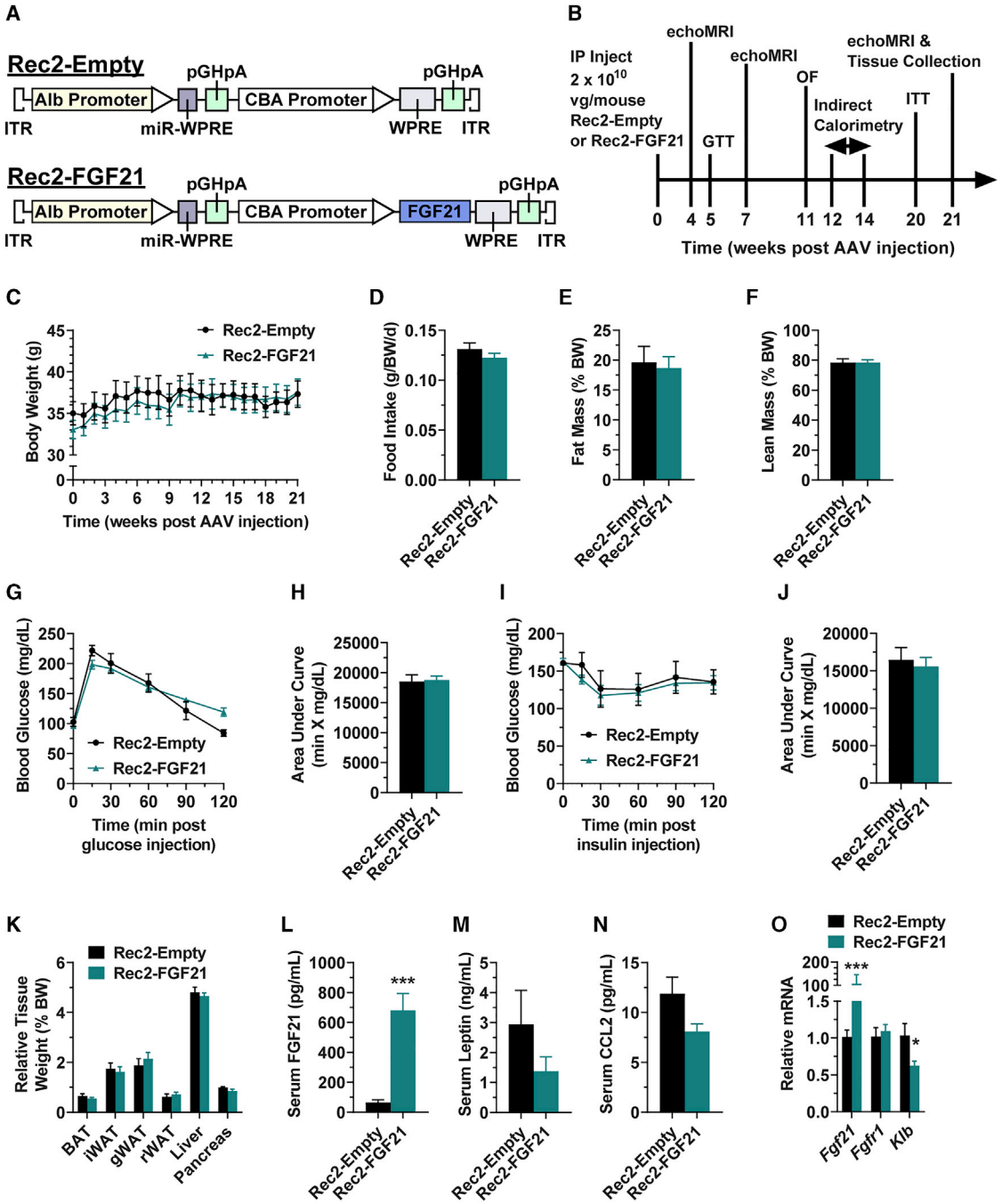

Figure 1. VAT-directed Rec2-FGF21 gene therapy under NCD conditions

(A) Vector schematic for Rec2-Empty and Rec2-FGF21. (B) Experimental timeline. (C) Body weights following rAAV administration. (D) Relative daily food intake. (E) Relative fat mass at 21 weeks post-rAAV-injection. (F) Relative lean mass at 21 weeks post-rAAV-injection. (G) Glucose tolerance test at 5 weeks post-rAAV-injection. (H) Glucose tolerance test area under the curve. (I) Insulin tolerance test at 20 weeks post-rAAV-injection. (J) Insulin tolerance test area under the curve. (K) Relative tissue weight at sacrifice. (L) Serum FGF21 at sacrifice. (M) Serum leptin at sacrifice. (N) Serum CCL2 at sacrifice (n = 4, Rec2-Empty; n = 7, Rec2-FGF21). (O) Gene expression profile of gWAT (n = 4, Rec2-Empty; n = 6, Rec2-FGF21). Data are means ± SEM. Sample size, Rec2-Empty, n = 4; Rec2-FGF21, n = 8 unless otherwise noted. +$p < 0.06$, *$p < 0.05$, **$p < 0.01$, ***$p < 0.001$.

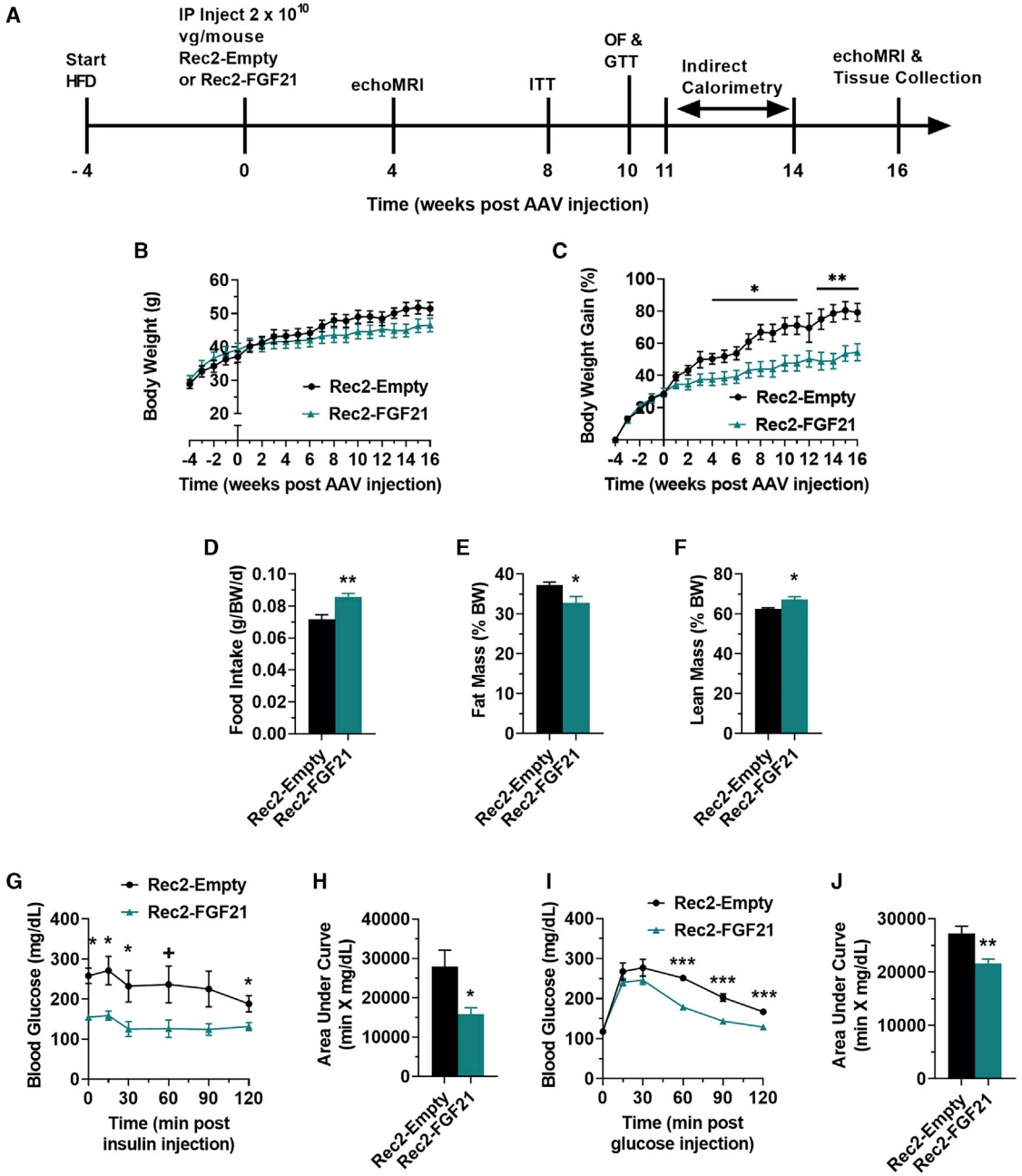

Figure 2. VAT-directed Rec2-FGF21 gene therapy in DIO mice

(A) Experimental timeline. (B) Body weights. (C) Percent change in body weight. (D) Relative daily food intake. (E) Relative fat mass at 16 weeks post-rAAV-injection. (F) Relative lean mass at 16 weeks post-rAAV-injection. (G) Insulin tolerance test at 8 weeks post-rAAV-injection (n = 7, Rec2-Empty; n = 6, Rec2-FGF21). (H) Insulin tolerance test area under the curve (n = 7, Rec2-Empty; n = 6, Rec2-FGF21). (I) Glucose tolerance test at 10 weeks post-rAAV-injection. (J) Glucose tolerance test area under the curve. Data are means ± SEM. Sample size, Rec2-Empty, n = 7; Rec2-FGF21, n = 7 unless otherwise noted. +$p < 0.06$, *$p < 0.05$, **$p < 0.01$, ***$p < 0.001$.

consumption (Figures 3A and 3B) and carbon dioxide expiration (Figures 3C and 3D), indicative of elevated energy expenditure consistent with previous observations following FGF21 gene therapy.[16] No differences were observed in RER (Figures 3E and 3F) or ambulation (Figures 3G and 3H). Together, these data indicate FGF21 gene therapy to the VAT resulted in improved systemic metabolism.

At 16 weeks post-AAV-injection, mice were sacrificed and tissues were collected. Rec2-FGF21 mice displayed reduced iWAT weight

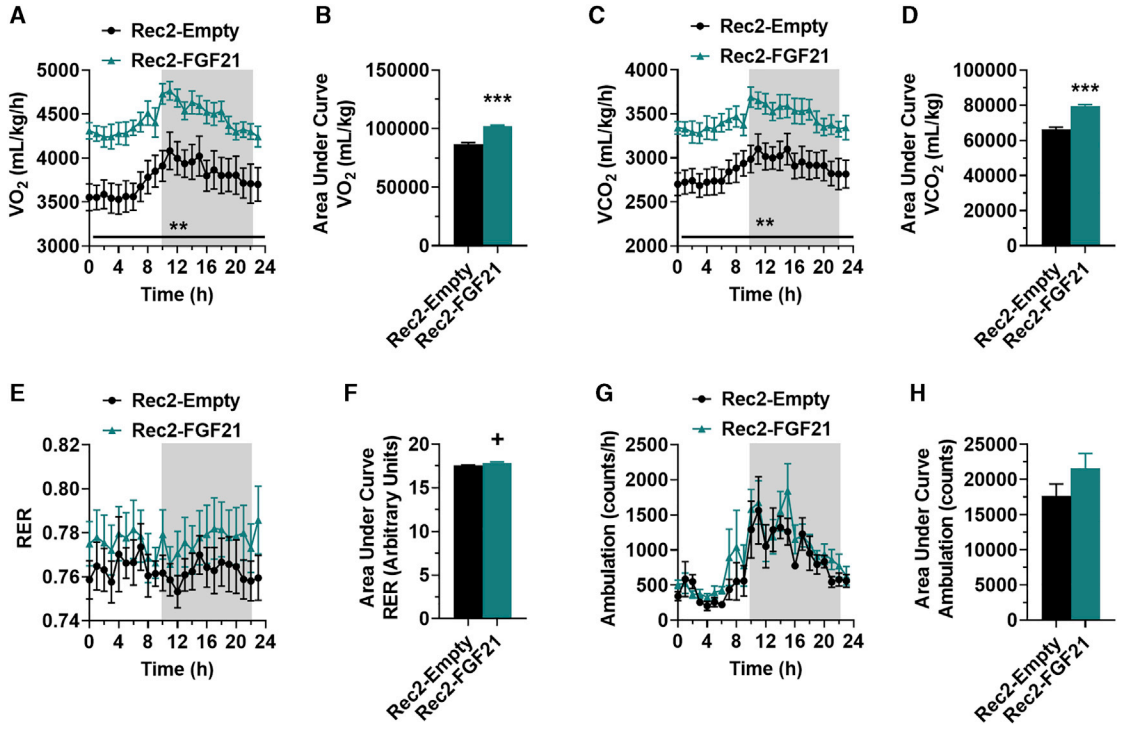

Figure 3. Indirect calorimetry of VAT-directed Rec2-FGF21 gene therapy in DIO mice

Shaded areas indicate dark phase. (A) Volume of O_2 consumption, normalized to body weight. (B) Area under curve of O_2 consumption. (C) Volume of CO_2 expiration, normalized to body weight. (D) Area under curve of CO_2 expiration. (E) Respiratory exchange ratio (RER). (F) Area under curve of RER. (G) Hourly ambulation measured by laser beam breaks. (H) Area under curve of ambulation. Data are means ± SEM. Sample size, Rec2-Empty, n = 6; Rec2-FGF21, n = 7. +$p < 0.06$, *$p < 0.05$, **$p < 0.01$, ***$p < 0.001$.

(Figure 4A) and relative tissue weight (Figure 4B). No differences were observed in the tissue weight or relative tissue weight of the virally treated gWAT (Figures 4A and 4B). Rec2-FGF21 mice additionally displayed a significant increase in relative tissue weight of gastrocnemius (Figure 4B). A large reduction in liver absolute weight and relative tissue weight was observed in the Rec2-FGF21 group (Figures 4C and 4D). Hepatic steatosis was alleviated in Rec2-FGF21 mice as measured by liver H&E staining (Figure 4E) and triglyceride quantification (Figure 4F). Of note, *Fgf21* overexpression was not observed in the liver, consistent with the liver-restricting nature of the dual-cassette AAV vector design (Figure 4G).

VAT-directed FGF21 gene therapy alters serum adipokine and inflammation markers in DIO mice

As expected, FGF21 was increased in the serum of Rec2-FGF21 mice (Figure 5A). Given this observation, we profiled various serum markers of metabolic function and inflammation to assess changes following FGF21 gene therapy.

Adiponectin is an adipokine that has been shown to connect FGF21 action in adipocytes to liver and skeletal muscle, thus improving insulin sensitivity, glucose homeostasis, and systemic metabolism.[2,39] Accordingly, there was a trend toward increased total adiponectin ($p = 0.08$) (Figure 5B) and significantly increased high-molecular-weight (HMW) adiponectin in the serum of Rec2-FGF21 mice (Figure 5C). The ratio of HMW adiponectin to total adiponectin has been described as an advanced marker of systemic metabolism and cardiac health.[40] Rec2-FGF21 mice displayed an increase in the HMW:total adiponectin ratio (Figure 5D).

Leptin is predominantly secreted by adipocytes and serves as a central-peripheral messenger to maintain energy homeostasis. Leptin production is positively correlated with adipose tissue mass and additionally has been described as a proinflammatory link between immune and neuroendocrine systems.[41] Rec2-FGF21 mice displayed approximately 70% reduction of serum leptin level (Figures 1C and 5E). No changes in serum fatty acids (Figure 5F), triglycerides (Figure 5G), or glucose (Figure 5H) were observed. A trending, but not significant ($p = 0.08$), decrease in serum insulin was observed (Figure 5I), indicative of a trend toward improved insulin sensitivity. No difference was observed in the HOMA-IR (homeostasis model assessment of insulin resistance) index of the two groups after a 4-h fast (Figure 5J).

We additionally profiled several serum proinflammatory cytokines and chemokines. Serum amyloid A (SAA) serves as a marker of inflammation and is thought to be tied to macrophage-related immunologic pathways.[42,43] We observed a strong trend of reduction of

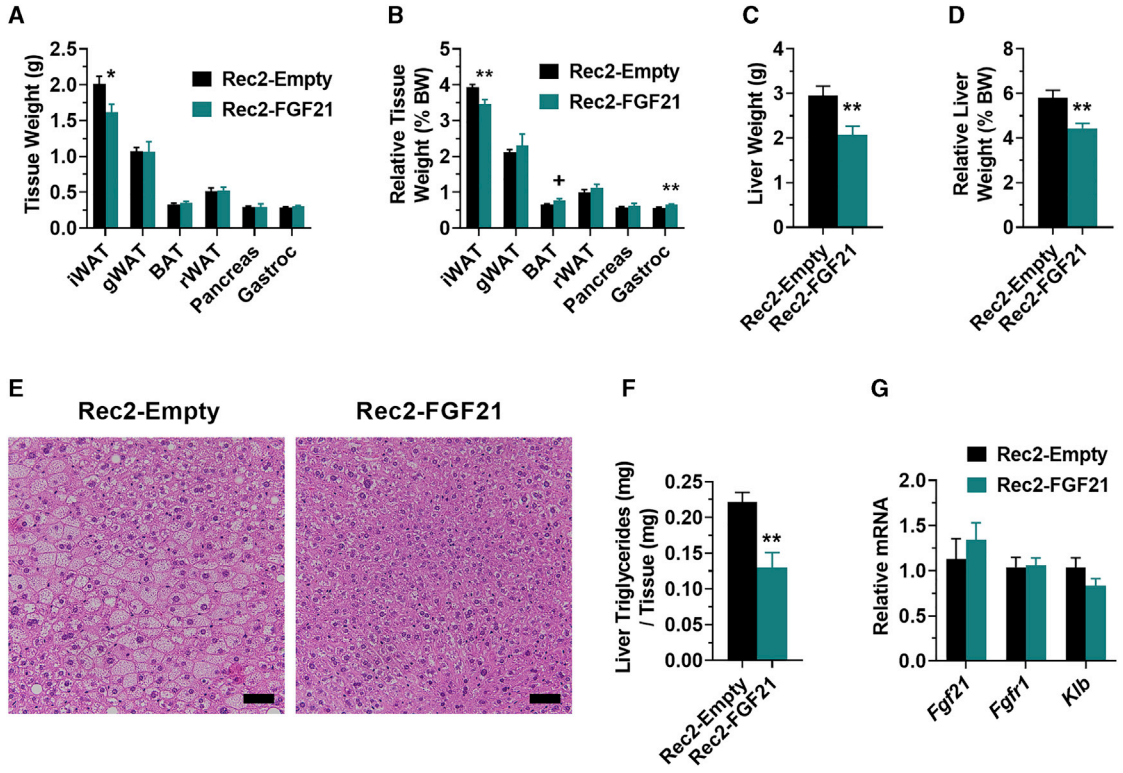

Figure 4. Gross tissues and liver analysis

(A) Tissue weights at sacrifice. (B) Relative tissue weights at sacrifice. (C) Liver weight at sacrifice. (D) Relative liver weight at sacrifice. (E) Representative H&E staining of liver tissue. Scale bar, 50 μm. (F) Hepatic triglycerides. (G) Gene expression profiling of liver tissue. Data are means ± SEM. Sample size, Rec2-Empty, n = 7; Rec2-FGF21, n = 7. +$p < 0.06$, *$p < 0.05$, **$p < 0.01$, ***$p < 0.001$.

SAA in the Rec2-FGF21 group as compared to controls (Figure 5K). Plasminogen activator inhibitor-1 (PAI-1) is involved in fibrinolysis and its elevation thought to contribute to vascular disease and inflammation in obese states.[44,45] PAI-1 levels were reduced in the Rec2-FGF21 group (Figure 5L), indicative of improved metabolic function and reduced inflammation. Serum CCL2 levels were reduced in the Rec2-FGF21 group (Figure 5M), indicative of decreased inflammation; these findings are additionally consistent with the observed improvements in insulin sensitivity.[46] No change in interleukin-1 beta (IL-1β) serum levels was observed (Figure 5N).

VAT-directed FGF21 gene therapy alters adipose and hypothalamic gene expression in DIO mice

In the gWAT, *Fgf21* was robustly overexpressed, with Rec2-FGF21-treated tissue showing a 40-fold increase over Rec2-Empty controls (Figure 6A). This overexpression was accompanied by a downregulation of FGF21 receptor genes, *Fgfr1* and *Klb* (Figure 6A). No significant differences were observed in two other FGF21 receptors, *Fgfr2* and *Fgfr3*. A significant downregulation of *Lep* (encoding leptin) was observed in Rec2-FGF21-treated gWAT, consistent with serum observations. No change in *Adipoq* (encoding adiponectin) was observed. Peroxisome proliferator-activated receptor gamma coactivator 1-alpha (PGC1-α, encoded by *Ppargc1a*), a transcriptional coactivator involved in mitochondrial biogenesis,[47] was significantly upregulated in Rec2-FGF21-treated gWAT, while no change in *Ucp1* (encoding uncoupling protein-1) was observed (Figure 6A). In addition, several markers of inflammation were assessed in the gWAT. *Ccl2* mRNA remained unchanged (Figure 6A), despite reduced serum levels. *Pai1* expression was reduced in the Rec2-FGF21 group, consistent with serum observations (Figure 6A). Two markers of inflammation involved in the NLRP3 inflammasome complex, *Casp1* (encoding caspase-1) and *Pycard* (encoding apoptosis-associated speck-like protein containing a CARD) were reduced in Rec2-FGF21-treated gWAT. No changes in macrophage markers *Il10* (encoding interleukin-10), *Arg1* (encoding arginase), *Mrc1* (encoding mannose receptor c-type 1), or *Clec10a* (encoding c-type lectin domain family 10 member A) were observed in the gWAT (Figure S5A).

We assessed gene expression in an additional VAT depot, the rWAT (Figure 6B). A robust 120-fold overexpression of *Fgf21* was observed in the Rec2-FGF21-treated rWAT. Despite this robust overexpression, no changes were observed in various adipokine and inflammation markers. In the iWAT—a nontargeted subcutaneous adipose depot—no changes in *Fgf21* or its receptors were observed (Figure 6C), consistent with the viral administration technique. In the iWAT, adipokine and mitochondrial markers remained unchanged.

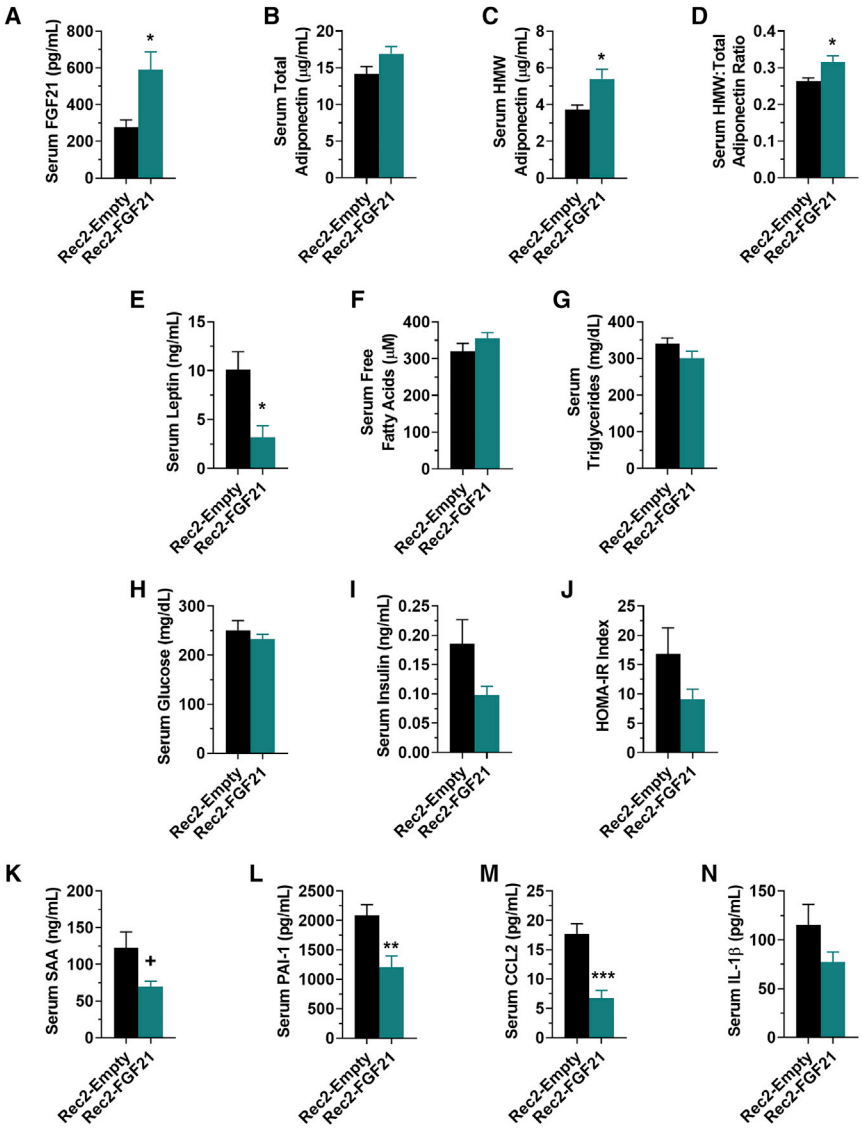

Figure 5. VAT-directed FGF21 gene therapy alters serum adipokine and inflammation markers in DIO mice

All serum measurements were taken at experiment endpoint. (A) Serum FGF21 (n = 6, Rec2-Empty; n = 7, Rec2-FGF21). (B) Serum total adiponectin (n = 5, Rec2-Empty; n = 6, Rec2-FGF21). (C) Serum high-molecular-weight (HMW) adiponectin (n = 5, Rec2-Empty; n = 6, Rec2-FGF21). (D) Serum ratio of HMW adiponectin to total adiponectin (n = 5, Rec2-Empty; n = 6, Rec2-FGF21). (E) Serum leptin (n = 6, Rec2-Empty; n = 7, Rec2-FGF21). (F) Serum-free fatty acids (n = 6, Rec2-Empty; n = 6, Rec2-FGF21). (G) Serum triglycerides (n = 5, Rec2-Empty; n = 5, Rec2-FGF21). (H) Serum glucose (n = 6, Rec2-Empty; n = 6, Rec2-FGF21). (I) Serum insulin (n = 7, Rec2-Empty; n = 6, Rec2-FGF21). (J) Homeostatic model of insulin resistance (HOMA-IR) score (n = 6, Rec2-Empty; n = 5, Rec2-FGF21). (K) Serum amyloid A (n = 6, Rec2-Empty; n = 7, Rec2-FGF21). (L) Serum PAI-1 (n = 6, Rec2-Empty; n = 5, Rec2-FGF21). (M) Serum CCL2 (n = 6, Rec2-Empty; n = 7, Rec2-FGF21). (N) Serum IL-1β (n = 6, Rec2-Empty; n = 5, Rec2-FGF21). Data are means ± SEM. +$p < 0.06$, *$p < 0.05$, **$p < 0.01$, ***$p < 0.001$.

Two markers of inflammation, *Ccl2* and *Pai1*, were downregulated in the Rec2-FGF21 group (Figure 6C). In the BAT, gene expression of *Fgf21* and its receptors remained unchanged (Figure 6D). Rec2-FGF21 mice displayed a reduction of *Lep* gene expression in the BAT, with no change in *Adipoq*. In the BAT, various markers of mitochondrial function, thermogenesis, and fatty acid synthesis/oxidation—including *Ppargc1a*, *Ucp1*, *Dio2* (encoding iodothyronine deiodinase 2), and *Ppara* (encoding peroxisome proliferator activated receptor alpha)—remained unchanged (Figure 6D). No transgene expression was found in pancreas or skeletal muscle. No changes in *Fgf21*, *Fgfr1*, or *Klb* were observed in the pancreas (data not shown) or the gastrocnemius (Figure S5B).

It is well documented that FGF21 acts centrally—through CRH—to induce energy expenditure, thermogenesis, and sympathetic nerve activity.[34–36] Given the observed improvements in systemic metabolic function, we measured hypothalamic gene expression of several neuroendocrine and inflammatory markers in the HFD cohort (Figure S5C). No changes in *Fgfr1* or *Klb* were observed. Hypothalamic *Crh* was upregulated, consistent with peripheral upregulation of FGF21.[34] *Insr* was upregulated, consistent with the observed serum insulin reduction in the Rec2-FGF21 treated group. No changes were observed in additional neuroendocrine markers, including *Obrb*, *Npy*, *Pomc*, and *TrkB-FL*. In contrast to Rec2-FGF21 treatment in NCD mice, no changes in a myriad of inflammation markers, including *Ccl2*, *Il1b*, *Ikbkb*, *Il18*, *Il33*, and *H2Ab1* were observed in HFD mice. Interestingly, we observed upregulation of *Tnfa* in the Rec2-FGF21 group.

VAT-directed FGF21 gene therapy reduces ATM inflammation in DIO mice

Under obese conditions, adipose tissue macrophages (ATMs) accumulate in VAT and exhibit a proinflammatory M1 polarization ($CD11c^+$, $CD206^-$), contributing to insulin resistance.[48] In contrast, lean animals present primarily with an M2-polarized state ($CD11c^-$, $CD206^+$), which is thought to protect adipocytes from inflammation.[48] As such, we isolated the stromal vascular fraction (SVF) from gWAT and performed fluorescence-activated cell sorting (FACS). Administration of Rec2-FGF21 resulted in distinct changes in ATM polarization within the VAT (Figure 7A). While no percentage changes in the total population of ATMs (Figure 7B) and M1-polarized populations (Figure 7C)

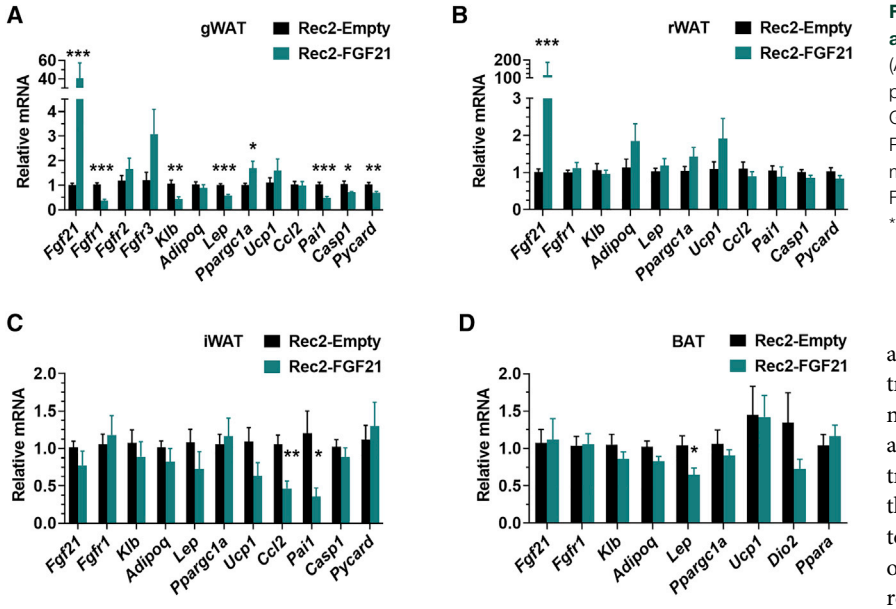

Figure 6. VAT-directed FGF21 gene therapy alters adipose gene expression in DIO mice

(A) Gene expression profile of gWAT. (B) Gene expression profile of rWAT. (C) Gene expression profile of iWAT. (D) Gene expression profile of BAT (n = 5, Rec2-Empty; n = 7, Rec2-FGF21 for *Ppargc1a*, *Dio2*, *Ppara* only). Data are means ± SEM. Sample size, Rec2-Empty, n = 7; Rec2-FGF21, n = 7 unless otherwise noted. +$p < 0.06$, *$p < 0.05$, **$p < 0.01$, ***$p < 0.001$.

were observed, a significant percentage increase in M2 polarization was observed in VAT of Rec2-FGF21 mice (Figure 7D). This change was accompanied by a significant percentage decrease in double-positive ($CD11c^+$, $CD206^+$) ATMs (Figure 7E). ATMs with this signature have been identified as sources of proinflammatory cytokines and are thought to be drivers of insulin resistance.[49] These data indicate that FGF21 gene therapy to the VAT reduced ATM inflammation and is associated with the observed improvements in insulin sensitivity and systemic metabolism. We additionally profiled other immune cell populations in the gWAT. No changes were observed in populations of natural killer T cells (Figure 7F), T cells (Figure 7G), or subpopulations of $CD4^+$ T cells (Figure 7H) and $CD8^+$ T cells (Figure 7I).

DISCUSSION

The present work provides evidence of a novel adipose-targeting, liver-restricting rAAV vector for long-term, specific transgene expression within VAT. Here, VAT depots were targeted using the adipo-trophic Rec2 serotype in tandem with a dual-cassette rAAV utilizing a liver-restricting element.[25] Combined, these techniques allow for a minimally invasive delivery system that is equivalent to direct fat injections. By utilizing the VAT as an FGF21 "factory" or "pump" to induce FGF21 in circulation, insulin resistance and obesity were reversed in BTBR mice. In additional, local and systemic obesity-associated inflammation was reduced.

Here, we report i.p. Rec2-FGF21 administration promotes a robust VAT-specific overexpression of FGF21 with no change in liver transgene expression. This technique builds upon an extensive report that highlighted the potential for FGF21 gene therapy to counter obesity and insulin resistance in HFD and *ob/ob* murine models.[16] Our technique differs in two important manners. First, the previous report used AAV8 serotype vector and target sequences for miR-122a and miR-1 to limit transgene expression in the liver and heart.[16] We used an engineered hybrid serotype Rec2 vector—which transduces adipose tissue more efficiently than the naturally occurring AAV8[24]—in combination with a dual-cassette design to restrict off-target liver transduction.[25] This study adds to the literature that characterizes the efficacy of this vector system to selectively transduce adipose tissue.[25,31,32] Second, Jimenez and colleagues[16] performed a laparotomy to directly administer their AAV8 vectors to VAT, whereas the technique presented here allows for non-invasive i.p. injections. In theory, our technique is clinic friendly and stresses the importance of developing minimally invasive administration techniques for widespread use of AAVs as therapeutic agents.

Functionally, our vectors performed similarly. VAT-specific overexpression of FGF21 in *ob/ob*[16] and BTBR mouse models resulted in increased serum FGF21, increased serum adiponectin, improved glycemia and insulinemia, improved insulin sensitivity, and reduced hepatic steatosis. The previous work found that FGF21 gene therapy to VAT reduced immunostaining of a macrophage marker, Mac2, and expression of F4/80.[16] Our work expands upon these observations, as we performed FACS to more comprehensively observe the immune populations residing in the AAV-treated gWAT, thus profiling ATM polarization and T cell subsets. Importantly, we discovered Rec2-FGF21 gene therapy altered ATM polarization toward a less-inflammatory state, characterized by an increase in anti-inflammatory M2 polarization ($CD11c^-$, $CD206^+$) and a decrease in proinflammatory double-positive ($CD11c^+$, $CD206^+$) ATMs. These ATM phenotypes have been shown to have causal links to lean states and improved insulin sensitivity.[48,49] Consistent with the favorable ATM polarization, Rec2-FGF21 administration downregulated the expression of proinflammatory cytokines, chemokines, and inflammasome components in treated gWAT. This gene signature was associated with significant reduction of cytokine and chemokine levels in circulation, suggesting alleviating VAT inflammation is sufficient to lessen systemic chronic inflammation—which, importantly, is implicated in various diseases beyond obesity and T2D. These observations warrant further investigation of VAT-targeted FGF21 gene therapy to treat cardiovascular diseases, non-alcoholic fatty liver disease, and certain types of cancer.

Adiponectin has been proposed as a messenger that links FGF21 actions in local adipocytes to liver and skeletal muscle.[2,39] FGF21

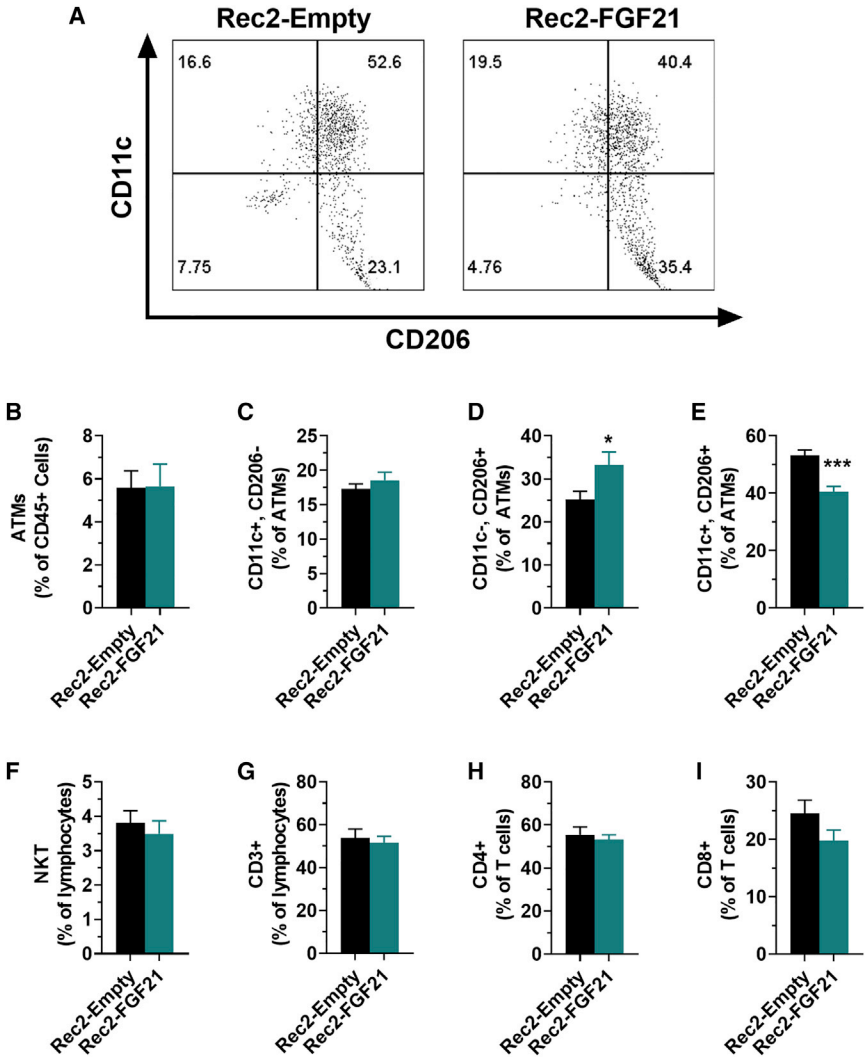

Figure 7. VAT-directed FGF21 gene therapy reduces ATM inflammation in DIO mice

(A) Representative FACS plot of ATMs in gWAT. (B) ATMs as a percentage of all $CD45^+$ cells. (C) Percentage of $CD11c^+$, $CD206^-$ ATMs. (D) Percentage of $CD11c^-$, $CD206^+$ ATMs. (E) Percentage of $CD11c^+$, $CD206^+$ ATMs. (F) Percentage of natural killer T cells. (G) Percentage of $CD3^+$ cells. (H) Percentage of $CD4^+$ T cells. (I) Percentage of $CD8^+$ T cells. Data are means ± SEM. Sample size (B–E), Rec2-Empty, n = 5; Rec2-FGF21, n = 7. Sample size (F–I), Rec2-Empty, n = 6; Rec2-FGF21, n = 7. +$p < 0.06$, *$p < 0.05$, **$p < 0.01$, ***$p < 0.001$.

treatment increases adiponectin secretion from adipocytes,[2,39] and adiponectin has been shown to promote M2 macrophage polarization.[50] Additionally, adiponectin has been shown to confer the effects of FGF21 on hepatic fatty acid oxidation and lipid clearance.[2] Interestingly, we observed reduced hepatic steatosis following VAT-directed gene therapy; this change was not due to increased hepatic FGF21 expression. We observed increased serum adiponectin following VAT-directed FGF21 gene therapy, providing one potential explanation for the observed reduction in hepatic triglycerides. While not the primary focus of this work, these findings highlight the importance of investigating tissue crosstalk following tissue-directed gene therapy and understanding mechanistic players in such processes.

In the BAT of the Rec2-FGF21-treated group, we observed no change in *Ucp1* expression or associated genes. Previous work has shown that FGF21 increases whole-body energy expenditure in ablated BAT and UCP-1 knockout mouse models,[51,52] suggesting FGF21 plays a role in UCP-1-independent thermogenic processes. In contrast to our data, the previous report showed that liver-directed administration of FGF21 gene therapy induced UCP-1 and browning in BAT.[16] Further work is needed to understand the mechanisms of FGF21 in UCP-1-dependent/-independent thermogenesis and to delineate whether tissue source of FGF21 (e.g., liver or adipose tissue) matters in such biological processes.

WAT depots vary in function and their responses to metabolic stimuli. WAT is broadly classified into two depots—VAT and subcutaneous adipose tissue. The former surrounds internal organs and is associated with insulin resistance, metabolic disease, and is thought to contribute to local/systemic inflammation.[21,53,54] The latter is found predominantly around the thighs and is associated with insulin sensitivity.[55] In the present work, we target VAT preferentially with Rec2-FGF21. i.p. administration of Rec2 vector did not result in transgene expression in subcutaneous iWAT. Interestingly, mild reductions in inflammation and relative tissue weight were observed in iWAT in absence of increased *Fgf21*, *Fgfr1*, and *Klb* expression. These results bring questions regarding adipose-adipose crosstalk and FGF21's role in mediating overall metabolic function. FGF21 has differential actions on various WAT depots; in subcutaneous adipose tissue, FGF21 regulates PGC1-α and browning in adaptive thermogenesis.[8] Furthermore, a recent report suggests that FGF21 induces transcriptomic changes associated with reduced subcutaneous adipose tissue weight.[56] Data on FGF21's specific roles in VAT are less conclusive and warrant further investigation. The AAV technology presented here provides one such method to further probe these depot-specific roles; two visceral adipose depots, gWAT and rWAT, displayed robust transgene expression with neglectable transgene expression in subcutaneous iWAT. Notably, growing evidence suggests incongruences between functional aspects of human and murine WAT depots[57–59]—careful experimental design and depot-specific techniques must be used to aid in translation of murine findings to human health.

BTBR mice are an inbred strain often used as a model of autism spectrum disorder (ASD). HFD is shown to exacerbate social deficiencies and cognitive rigidity in BTBR mice.[60] Moreover, BTBR mice display aberrant immune responses compared to more sociable C57BL/6 mice, characterized by higher anti-brain antibodies, elevated expression of cytokines in the brain—particularly IL-33 and IL-18, and an increased proportion of MHC II-expressing microglial cells. It is proposed that the constitutive neuroinflammation indicates an autoimmune profile contributing to their aberrant behaviors.[61] Rec2-FGF21 treatment led to downregulation of a cluster of immune-modulatory genes in the hypothalamus (*Il33*, *Il1b*, *Ccl2*, *Tnfa*, *Ikbkb*, *H2Ab1*; Figure S3) under NCD conditions, although metabolic outcomes were unremarkable. The impact of adipose-targeted FGF21 treatment on neuroinflammation, behaviors, and the underlying mechanisms warrant future investigation. Another unexpected finding is that the HFD-induced hypothalamic neuroinflammation in C57BL/6 mice was absent in the BTBR mice, although BTBR mice remain more prone to DIO. These observations warrant further work on (1) the aberrant neuroendocrinological and neuroimmunological differences between the insulin-resistant, ASD-like BTBR model and sociable strains, and (2) assessments of the potential benefits of FGF21 treatment beyond metabolic outcomes.

From a therapeutic standpoint, FGF21 AAVs provide several advantages to administration of native FGF21 peptide, analogs, and/or mimetics; such therapeutics require repeated administration, patient adherence, and may be subject to immunological concerns stemming from use of exogenous proteins. In contrast, FGF21 gene therapy via AAV constructs would require but a single administration for long-term transgene persistence. AAV-FGF21 vectors have the additional advantage of producing the wild-type protein, which is easily recognized by canonical FGF21 signaling pathways and has a reduced likelihood of inducing peptide-related adverse immune responses.

It is important to consider the use indications for FGF21 gene-therapy vectors, analogs, and mimetics. Importantly, we observe limited alterations in systemic metabolism following VAT-directed FGF21 gene therapy in mice on NCD. At this time, the use of AAV FGF21 techniques would not be indicated for use in non-obese individuals like the ones reported in the NCD study (Figure 1). Indeed, the overwhelming majority of preclinical and clinical trials for FGF21 gene therapy, analogs, and mimetics are for obese and/or diabetic individuals.[62] Some have considered aging as an indication for FGF21-related therapeutics. Davidsohn and colleagues[17] recently reported a combination gene therapy based on 3 longevity-associated genes—including FGF21—to treat multiple age-related diseases. Adipose tissue dysfunction is thought to be a key driver of aging, leading to a systemic proinflammatory state and multi-organ dysfunction. The related pathophysiology of age-related systemic functional decline often mirrors the pathologies related to obesity.[63] Accordingly, we have initiated a long-term study to examine VAT-directed FGF21 gene therapy on the effects of healthspan and lifespan in middle-aged mice.

In summary, AAV-mediated gene therapy is increasingly attractive as a strategy to fight obesity and metabolic diseases.[64,65] Excessive adiposity is a risk factor for T2D, metabolic syndrome, inflammation, and certain types of cancer.[66–70] VAT is a prime therapeutic target due to its nature as a secretory organ; adipokines can be harnessed to induce local and systemic improvements in metabolic and immune health.[71–73] Our study combines an engineered AAV serotype, liver-restricting design, and i.p. administration techniques to provide an example of VAT-targeted gene therapy. Currently, the vast majority of peripheral gene therapies target liver or muscle; the advantages and drawbacks of using these tissues as targets are well characterized.[74] In contrast, the advantages and disadvantages of adipose tissue as a targeting tissue remain largely unknown and warrant further investigation. The recent development of AAV vectors with improved adipose tropism and restriction of off-target transduction paves ways to investigate the long-term transgene expression, local and systemic immune responses, therapeutic efficacy, and safety profile of these vectors in adipose tissue.[75] New AAV administration techniques and bioengineering projects will be essential to increase specificity and efficacy of targeted gene therapies.[74,76]

MATERIALS AND METHODS

Animals

BTBR (Jackson Laboratory #002282) mice were obtained and bred in-house. Mice were housed in temperature (22°C –23°C) and humidity (30%–70%) controlled rooms under a 12-h:12-h light:dark cycle. All animal experiments were in accordance with the regulations of The Ohio State University's Institutional Animal Care and Use Committee.

NCD mice

Adult male BTBR mice (16–20 weeks old) were placed on NCD (11% fat, caloric density 3.4 kcal/g, Teklad). At baseline, mice were randomized to create two groups (n = 4, Rec2-Empty; and n = 8, Rec2-FGF21) that had no significant differences in age, body weight, fat mass percentage, or lean mass percentage. Following randomization, mice were administered rAAV vectors as described below. Mice were maintained on NCD for the remainder of the study, having *ad libitum* access to food and water. Body weights were monitored on a weekly basis. *In vivo* measurements occurred according to the timeline in Figure 1B.

DIO mice

Adult male BTBR mice (13–19 weeks old) were placed on HFD (60% kcal from lard; Research Diets #D12492). After 4 weeks of HFD, mice were randomized to create two groups (n = 7, Rec2-Empty; and n = 7, Rec2-FGF21) that had no significant differences in age, body weight, fat mass percentage, or lean mass percentage. Following randomization, mice were administered rAAV vectors as described below. Mice were maintained on HFD for the remainder of the study, having *ad libitum* access to food and water. Body weights were monitored on a weekly basis. *In vivo* measurements occurred according to the timeline in Figure 2A.

rAAV design and administration

Adipo-trophic rAAV serotype Rec2 vectors contained two expression cassettes. The first cassette consisted of the cytomegalovirus (CMV) enhancer and chicken β-actin (CBA) promoter, FGF21 transgene, WPRE, and bovine growth hormone poly(A) (Rec2-FGF21; Figure 1A). The second cassette encoded a microRNA targeting the WPRE sequence driven by basic albumin promoter to limit transgene expression in the liver. This liver-restricting dual cassette was previously described and verified.[25] The empty control vector (Rec2-Empty) lacked a transgene insertion in the multiple cloning sites. Rec2 serotype specificity, transduction efficacy in adipose tissue, and packaging were previously detailed elsewhere.[24,77,78] Rec2-Empty and Rec2-FGF21 rAAV vectors (2×10^{10} vg) were administered to mice via i.p. injections (in 150 μL AAV buffer).

EchoMRI

EchoMRI was utilized to measure body composition of fat and lean mass in live mice without anesthesia. Body composition analysis was performed with an echoMRI 3-in-1 analyzer at the Small Animal Imaging Core of the Dorothy M. Davis Heart & Lung Research Institute, The Ohio State University. Fat, lean, free water, and total water mass were measured by the echoMRI machine and then normalized to total body weight as measured 10 min prior to the scan.

ITT

Mice were injected i.p. with an insulin solution (1.5 U insulin per kg body weight) under non-fasting conditions. Blood was obtained from the tail at baseline, 15, 30, 60, 90, and 120 min after insulin injection. Blood glucose concentrations were measured with a portable glucose meter (Bayer Contour Next).

OF test

Mice were individually placed into the center of an open square arena (60 × 60 cm, enclosed by walls of 48 cm). Each mouse was allowed to explore the arena for 10 min, during which time and locomotion—in the center and the periphery of the OF—was recorded and analyzed via TopScan (CleverSys) software. Between each trial, the arena was cleaned with Opticide to remove odor cues.

GTT

Mice were injected i.p. with glucose solution (1.0 g glucose per kg body weight) after a 17-h overnight fast. Blood was obtained from the tail at baseline, 15, 30, 60, 90, and 120 min after glucose injection. Blood glucose concentrations were measured with a portable glucose meter (Bayer Contour Next).

Indirect calorimetry

Mice underwent indirect calorimetry using a comprehensive laboratory animal monitoring system (CLAMS; Columbus Instruments, Columbus, OH, USA). Mice were singly housed and had ample access to HFD and water. In our experience, BTBR mice have difficulty using novel water lixits. As such, mice were additionally supplemented with HydroGel cups (Clear H_2O #70-01-5022). Mice were allowed to habituate for 16–18 h and then various physiological and behavioral parameters (VO_2, VCO_2, RER, heat, and ambulation) were recorded at room temperature for 24 h. Mice were returned to their home cage after indirect calorimetry was performed.

Food intake

For the NCD experiment mice, weekly food intake was measured at the cage level and normalized to body weight and the number of mice per cage. Due to worries of food loss stemming from the physical consistency of HFD, the HFD mice were singly housed for 72 h. Food intake was measured every 24 h to provide three replicate measurements of daily intake per mouse. Measurements were normalized to body weight. HFD mice were returned to their home cages following food intake assessments.

Serum and tissue collection

Mice were euthanized and tissues were collected at 21 weeks post-injection (NCD mice) and 16 weeks post-injection (HFD mice). Trunk blood was collected at 10:00 following a 4-h fast. Blood was allowed to clot on ice for at least 30 min before centrifugation at 10,000 rpm for 10 min at 4°C. The serum component was collected and stored at −20°C until further analysis. Tissues were either fixed as described below or flash frozen and stored at −80°C until further analysis. Fat depots were identified, collected as described elsewhere,[79] and normalized to body weight as measured 10 min prior to euthanasia.

Histology

At sacrifice, portions of liver and adipose tissues were fixed in 10% formalin (w/v) for 48–72 h and then dehydrated with 70% ethanol. Tissues were embedded in paraffin, sectioned, and H&E stained by the Comparative Pathology and Mouse Phenotyping and Histology/Immunohistochemistry (CPMPSR) core of The Ohio State University Comprehensive Cancer Center. Tissue sections were imaged at 20× magnification using an Olympus BX43 microscope with an Olympus SC30 color camera attachment and Olympus cellSens software.

Hepatic triglyceride quantification

Lipids were extracted from liver tissue by chloroform/methanol (2:1 v/v), followed by rinses in 50 mM NaCl and $CaCl_2$ (0.36 M)/methanol (1:1 v/v).[80] Hepatic triglyceride quantification was performed with a Caymen Chemical triglyceride assay kit (#10010303).

Quantitative real-time PCR

Total RNA was isolated from adipose tissue using the RNeasy lipid kit plus RNase-free DNase treatment (QIAGEN #74804). First-strand cDNA was generated using TaqMan reverse transcription reagent (Applied Biosystems #N8080234). Quantitative real-time PCR was performed using power SYBR green PCR master mix (Applied Biosystems #A25742) on a StepOnePlus real-time PCR system (Applied Biosystems). Primers were designed to detect the following genes: *Adipoq*, *Arg1*, *Casp1*, *Ccl2*, *Clec10a*, *Crh*, *Dio2*, *Fgf21*, *Fgfr1*, *Fgfr2*, *Fgfr3*, *H2Ab1*, *Ikbkb*, *Il10*, *Il18*, *Il1b*, *Il33*, *Insr*, *Klb*, *Lep*, *Mrc1*, *Npy*,

Obrb, *Pai1*, *Pomc*, *Ppara*, *Ppargc1a*, *Pycard*, *Tnfa*, *TrkB-FL*, and *Ucp1* (Table S1). Data were calibrated to endogenous control *Actb* or *36B4* (adipose), *Ppia* (liver), *Hprt* (hypothalamus), *Gapdh* (muscle), and the relative gene expression was quantified using the $2^{-\Delta\Delta CT}$ method.[81]

Serum analysis

R&D Systems DuoSet ELISA kits were used to assay serum FGF21 (#DY3057), leptin (#DY498), SAA (#DY2948), PAI-1 (#DY3828), CCL2 (#DY479), and IL-1β (#DY401). Cayman Chemical assay kits were used to assay serum triglycerides (#10010303), free fatty acids (#700310), and glucose (#10009582). ALPCO ELISA kits were used to assay total/HMW adiponectin (#47-ADPMS-E01) and insulin (#80-INSMSU-E01). HOMA-IR index was calculated as (fasting serum glucose [mmol/L] × fasting serum insulin [pmol/L]/22.5) as described elsewhere.[82]

Isolation of adipose SVF and FACS

Samples of gWAT were minced into small pieces in Kreb-Ringer HEPES buffer (pH 7.4). Collagenase (1 mg/mL, Sigma #C6885) was added and incubated for 40 min at 37°C with shaking. The mixture was centrifuged to separate the floating adipocytes from the SVF. The SVF pellet was treated with ammonium chloride solution to lyse the red blood cells, then washed and resuspended in FACS buffer. 70-μM strainers were used to obtain a single-cell suspension. SVF cells were stained with fluorescent-dye-conjugated antibodies for 20 min. The antibodies used for flow cytometry immunophenotyping are listed in Table S2. Cell events were acquired using LSRII flow cytometry (BD Biosciences), and the results were analyzed using FlowJo v10 software (Tree Star).

Statistical analysis

Data are expressed as mean ± SEM. GraphPad Prism 7 software (GraphPad, La Jolla, CA, USA) and SPSS Statistics v25.0.0.0 (IBM, Armonk, NY, USA) were used to analyze data. Student's t tests were performed for all data except time course data. Mixed-model ANOVAs were used to analyze time course data (weekly body weights, GTTs, ITTs, and indirect calorimetry time measurements). Results of the between-group analyses are reported in the associated figures for weekly body weights and indirect calorimetry time measurements. Results of the pairwise comparisons are reported in the GTT and ITT graphs.

SUPPLEMENTAL INFORMATION

Supplemental Information can be found online at https://doi.org/10.1016/j.omtm.2020.12.011.

ACKNOWLEDGMENTS

We would like to thank Amber A. Boardman and Quais N. Hassan II for technical assistance. This work was supported by NIH grants AG041250, CA166590, and CA163640, as well as internal funding from The Ohio State University Comprehensive Cancer Center.

AUTHOR CONTRIBUTIONS

N.J.Q. and R.B. designed the studies, carried out the research, interpreted the results, and wrote the manuscript. W.H. designed the studies, carried out the research, and interpreted the results. R.X. and B.A. carried out the research and interpreted the results. L.C. conceived the concept, designed the studies, interpreted the results, and wrote the manuscript.

DECLARATION OF INTERESTS

L.C. and W.H. are inventors of a provisional patent application related to the liver-restricting AAV vector. All other authors declare no conflicts of interest.

REFERENCES

1. Véniant, M.M., Hale, C., Helmering, J., Chen, M.M., Stanislaus, S., Busby, J., Vonderfecht, S., Xu, J., and Lloyd, D.J. (2012). FGF21 promotes metabolic homeostasis via white adipose and leptin in mice. PLoS ONE *7*, e40164.

2. Lin, Z., Tian, H., Lam, K.S., Lin, S., Hoo, R.C., Konishi, M., Itoh, N., Wang, Y., Bornstein, S.R., Xu, A., and Li, X. (2013). Adiponectin mediates the metabolic effects of FGF21 on glucose homeostasis and insulin sensitivity in mice. Cell Metab. *17*, 779–789.

3. Chen, W., Hoo, R.L., Konishi, M., Itoh, N., Lee, P.C., Ye, H.Y., Lam, K.S., and Xu, A. (2011). Growth Hormone Induces Hepatic Production of Fibroblast Growth Factor 21 through a Mechanism Dependent on Lipolysis in Adipocytes. J. Biol. Chem *286*, 34559–34566.

4. Ding, X., Boney-Montoya, J., Owen, B.M., Bookout, A.L., Coate, K.C., Mangelsdorf, D.J., and Kliewer, S.A. (2012). βKlotho is required for fibroblast growth factor 21 effects on growth and metabolism. Cell Metab. *16*, 387–393.

5. Adams, A.C., Yang, C., Coskun, T., Cheng, C.C., Gimeno, R.E., Luo, Y., and Kharitonenkov, A. (2012). The breadth of FGF21's metabolic actions are governed by FGFR1 in adipose tissue. Mol. Metab. *2*, 31–37.

6. Kharitonenkov, A., Shiyanova, T.L., Koester, A., Ford, A.M., Micanovic, R., Galbreath, E.J., Sandusky, G.E., Hammond, L.J., Moyers, J.S., Owens, R.A., et al. (2005). FGF-21 as a novel metabolic regulator. J. Clin. Invest. *115*, 1627–1635.

7. Chau, M.D.L., Gao, J., Yang, Q., Wu, Z., and Gromada, J. (2010). Fibroblast growth factor 21 regulates energy metabolism by activating the AMPK–SIRT1–PGC-1α pathway. Proc. Natl. Acad. Sci. USA *107*, 12553–12558.

8. Fisher, F.M., Kleiner, S., Douris, N., Fox, E.C., Mepani, R.J., Verdeguer, F., Wu, J., Kharitonenkov, A., Flier, J.S., Maratos-Flier, E., and Spiegelman, B.M. (2012). FGF21 regulates PGC-1α and browning of white adipose tissues in adaptive thermogenesis. Genes Dev. *26*, 271–281.

9. Fisher, F.M., and Maratos-Flier, E. (2016). Understanding the Physiology of FGF21. Annu. Rev. Physiol. *78*, 223–241.

10. Coskun, T., Bina, H.A., Schneider, M.A., Dunbar, J.D., Hu, C.C., Chen, Y., Moller, D.E., and Kharitonenkov, A. (2008). Fibroblast growth factor 21 corrects obesity in mice. Endocrinology *149*, 6018–6027.

11. Berglund, E.D., Li, C.Y., Bina, H.A., Lynes, S.E., Michael, M.D., Shanafelt, A.B., Kharitonenkov, A., and Wasserman, D.H. (2009). Fibroblast growth factor 21 controls glycemia via regulation of hepatic glucose flux and insulin sensitivity. Endocrinology *150*, 4084–4093.

12. Kharitonenkov, A., and Adams, A.C. (2013). Inventing new medicines: The FGF21 story. Mol. Metab. *3*, 221–229.

13. Gaich, G., Chien, J.Y., Fu, H., Glass, L.C., Deeg, M.A., Holland, W.L., Kharitonenkov, A., Bumol, T., Schilske, H.K., and Moller, D.E. (2013). The effects of LY2405319, an FGF21 analog, in obese human subjects with type 2 diabetes. Cell Metab. *18*, 333–340.

14. Talukdar, S., Zhou, Y., Li, D., Rossulek, M., Dong, J., Somayaji, V., Weng, Y., Clark, R., Lanba, A., Owen, B.M., et al. (2016). A long-acting FGF21 molecule, PF-05231023, decreases body weight and improves lipid profile in non-human primates and type 2 diabetic subjects. Cell Metab. *23*, 427–440.

15. Kim, A.M., Somayaji, V.R., Dong, J.Q., Rolph, T.P., Weng, Y., Chabot, J.R., Gropp, K.E., Talukdar, S., and Calle, R.A. (2017). Once-weekly administration of a long-acting fibroblast growth factor 21 analogue modulates lipids, bone turnover markers, blood pressure and body weight differently in obese people with hypertriglyceridaemia and in non-human primates. Diabetes Obes. Metab. *19*, 1762–1772.

16. Jimenez, V., Jambrina, C., Casana, E., Sacristan, V., Muñoz, S., Darriba, S., Rodó, J., Mallol, C., Garcia, M., León, X., et al. (2018). FGF21 gene therapy as treatment for obesity and insulin resistance. EMBO Mol. Med. *10*, e8791.

17. Davidsohn, N., Pezone, M., Vernet, A., Graveline, A., Oliver, D., Slomovic, S., Punthambaker, S., Sun, X., Liao, R., Bonventre, J.V., and Church, G.M. (2019). A single combination gene therapy treats multiple age-related diseases. Proc. Natl. Acad. Sci. USA *116*, 23505–23511.

18. Deyle, D.R., and Russell, D.W. (2009). Adeno-associated virus vector integration. Curr. Opin. Mol. Ther. *11*, 442–447.

19. Verdera, H.C., Kuranda, K., and Mingozzi, F. (2020). AAV Vector Immunogenicity in Humans: A Long Journey to Successful Gene Transfer. Mol. Ther. *28*, 723–746.

20. Trayhurn, P., and Beattie, J.H. (2001). Physiological role of adipose tissue: white adipose tissue as an endocrine and secretory organ. Proc. Nutr. Soc. *60*, 329–339.

21. Wronska, A., and Kmiec, Z. (2012). Structural and biochemical characteristics of various white adipose tissue depots. Acta Physiol. (Oxf. *205*, 194–208.

22. Wozniak, S.E., Gee, L.L., Wachtel, M.S., and Frezza, E.E. (2009). Adipose tissue: the new endocrine organ? A review article. Dig. Dis. Sci. *54*, 1847–1856.

23. Cristancho, A.G., and Lazar, M.A. (2011). Forming functional fat: a growing understanding of adipocyte differentiation. Nat. Rev. Mol. Cell Biol. *12*, 722–734.

24. Liu, X., Magee, D., Wang, C., McMurphy, T., Slater, A., During, M., and Cao, L. (2014). Adipose tissue insulin receptor knockdown via a new primate-derived hybrid recombinant AAV serotype. Mol. Ther. Methods Clin. Dev. *1*, 8.

25. Huang, W., Liu, X., Queen, N.J., and Cao, L. (2017). Targeting Visceral Fat by Intraperitoneal Delivery of Novel AAV Serotype Vector Restricting Off-Target Transduction in Liver. Mol. Ther. Methods Clin. Dev. *6*, 68–78.

26. Huang, W., McMurphy, T., Liu, X., Wang, C., and Cao, L. (2016). Genetic Manipulation of Brown Fat Via Oral Administration of an Engineered Recombinant Adeno-associated Viral Serotype Vector. Mol. Ther *24*, 1062–1069.

27. Zhu, Y., Gao, Y., Tao, C., Shao, M., Zhao, S., Huang, W., Yao, T., Johnson, J.A., Liu, T., Cypess, A.M., et al. (2016). Connexin 43 Mediates White Adipose Tissue Beiging by Facilitating the Propagation of Sympathetic Neuronal Signals. Cell Metab. *24*, 420–433.

28. Ng, R., Hussain, N.A., Zhang, Q., Chang, C., Li, H., Fu, Y., Cao, L., Han, W., Stunkel, W., and Xu, F. (2017). miRNA-32 Drives Brown Fat Thermogenesis and Trans-activates Subcutaneous White Fat Browning in Mice. Cell Rep. *19*, 1229–1246.

29. Zhang, Y., Xie, L., Gunasekar, S.K., Tong, D., Mishra, A., Gibson, W.J., Wang, C., Fidler, T., Marthaler, B., Klingelhutz, A., et al. (2017). SWELL1 is a regulator of adipocyte size, insulin signalling and glucose homeostasis. Nat. Cell Biol. *19*, 504–517.

30. Siu, J.J., Queen, N.J., Huang, W., Yin, F.Q., Liu, X., Wang, C., McTigue, D.M., and Cao, L. (2017). Improved gene delivery to adult mouse spinal cord through the use of engineered hybrid adeno-associated viral serotypes. Gene Ther. *24*, 361–369.

31. Xiao, R., Mansour, A.G., Huang, W., Chrislip, L.A., Wilkins, R.K., Queen, N.J., Youssef, Y., Mao, H.C., Caligiuri, M.A., and Cao, L. (2019). Adipocytes: A Novel Target for IL-15/IL-15Rα Cancer Gene Therapy. Mol. Ther *27*, 922–932.

32. Huang, W., Queen, N.J., McMurphy, T.B., Ali, S., and Cao, L. (2019). Adipose PTEN regulates adult adipose tissue homeostasis and redistribution via a PTEN-leptin-sympathetic loop. Mol. Metab. *30*, 48–60.

33. Flowers, J.B., Oler, A.T., Nadler, S.T., Choi, Y., Schueler, K.L., Yandell, B.S., Kendziorski, C.M., and Attie, A.D. (2007). Abdominal obesity in BTBR male mice is associated with peripheral but not hepatic insulin resistance. Am. J. Physiol. Endocrinol. Metab *292*, E936–E945.

34. Owen, B.M., Ding, X., Morgan, D.A., Coate, K.C., Bookout, A.L., Rahmouni, K., Kliewer, S.A., and Mangelsdorf, D.J. (2014). FGF21 acts centrally to induce sympathetic nerve activity, energy expenditure, and weight loss. Cell Metab. *20*, 670–677.

35. Douris, N., Stevanovic, D.M., Fisher, F.M., Cisu, T.I., Chee, M.J., Nguyen, N.L., Zarebidaki, E., Adams, A.C., Kharitonenkov, A., Flier, J.S., et al. (2015). Central fibroblast growth factor 21 browns white fat via sympathetic action in male mice. Endocrinology *156*, 2470–2481.

36. Liang, Q., Zhong, L., Zhang, J., Wang, Y., Bornstein, S.R., Triggle, C.R., Ding, H., Lam, K.S.L., and Xu, A. (2014). FGF21 Maintains Glucose Homeostasis by Mediating the Cross Talk Between Liver and Brain During Prolonged Fasting. Diabetes *63*, 4064–4075.

37. Ogawa, Y., Kurosu, H., Yamamoto, M., Nandi, A., Rosenblatt, K.P., Goetz, R., Eliseenkova, A.V., Mohammadi, M., and Kuro-o, M. (2007). BetaKlotho is required for metabolic activity of fibroblast growth factor 21. Proc. Natl. Acad. Sci. USA *104*, 7432–7437.

38. Bookout, A.L., de Groot, M.H., Owen, B.M., Lee, S., Gautron, L., Lawrence, H.L., Ding, X., Elmquist, J.K., Takahashi, J.S., Mangelsdorf, D.J., and Kliewer, S.A. (2013). FGF21 regulates metabolism and circadian behavior by acting on the nervous system. Nat. Med. *19*, 1147–1152.

39. Holland, W.L., Adams, A.C., Brozinick, J.T., Bui, H.H., Miyauchi, Y., Kusminski, C.M., Bauer, S.M., Wade, M., Singhal, E., Cheng, C.C., et al. (2013). An FGF21-adiponectin-ceramide axis controls energy expenditure and insulin action in mice. Cell Metab. *17*, 790–797.

40. Aso, Y., Yamamoto, R., Wakabayashi, S., Uchida, T., Takayanagi, K., Takebayashi, K., Okuno, T., Inoue, T., Node, K., Tobe, T., et al. (2006). Comparison of Serum High-Molecular Weight (HMW) Adiponectin With Total Adiponectin Concentrations in Type 2 Diabetic Patients With Coronary Artery Disease Using a Novel Enzyme-Linked Immunosorbent Assay to Detect HMW Adiponectin. Diabetes *55*, 1954–1960.

41. Abella, V., Scotece, M., Conde, J., Pino, J., Gonzalez-Gay, M.A., Gómez-Reino, J.J., Mera, A., Lago, F., Gómez, R., and Gualillo, O. (2017). Leptin in the interplay of inflammation, metabolism and immune system disorders. Nat. Rev. Rheumatol. *13*, 100–109.

42. Gabay, C., and Kushner, I. (1999). Acute-Phase Proteins and Other Systemic Responses to Inflammation. N. Engl. J. Med *340*, 448–454.

43. Sack, G.H., Jr. (2018). Serum amyloid A - a review. Mol. Med. *24*, 46.

44. Shimomura, I., Funahashi, T., Takahashi, M., Maeda, K., Kotani, K., Nakamura, T., Yamashita, S., Miura, M., Fukuda, Y., Takemura, K., et al. (1996). Enhanced expression of PAI-1 in visceral fat: possible contributor to vascular disease in obesity. Nat. Med. *2*, 800–803.

45. Juhan-Vague, I., Alessi, M.-C., Mavri, A., and Morange, P.E. (2003). Plasminogen activator inhibitor-1, inflammation, obesity, insulin resistance and vascular risk. J. Thromb. Haemost *1*, 1575–1579.

46. Tateya, S., Tamori, Y., Kawaguchi, T., Kanda, H., and Kasuga, M. (2010). An increase in the circulating concentration of monocyte chemoattractant protein-1 elicits systemic insulin resistance irrespective of adipose tissue inflammation in mice. Endocrinology *151*, 971–979.

47. Mootha, V.K., Lindgren, C.M., Eriksson, K.-F., Subramanian, A., Sihag, S., Lehar, J., Puigserver, P., Carlsson, E., Ridderstråle, M., Laurila, E., et al. (2003). PGC-1α-responsive genes involved in oxidative phosphorylation are coordinately downregulated in human diabetes. Nat. Genet. *34*, 267–273.

48. Lumeng, C.N., Bodzin, J.L., and Saltiel, A.R. (2007). Obesity induces a phenotypic switch in adipose tissue macrophage polarization. J. Clin. Invest. *117*, 175–184.

49. Wentworth, J.M., Naselli, G., Brown, W.A., Doyle, L., Phipson, B., Smyth, G.K., Wabitsch, M., O'Brien, P.E., and Harrison, L.C. (2010). Pro-Inflammatory CD11c+CD206+ Adipose Tissue Macrophages Are Associated With Insulin Resistance in Human Obesity. Diabetes *59*, 1648–1656.

50. Ohashi, K., Parker, J.L., Ouchi, N., Higuchi, A., Vita, J.A., Gokce, N., Pedersen, A.A., Kalthoff, C., Tullin, S., Sams, A., et al. (2010). Adiponectin promotes macrophage polarization toward an anti-inflammatory phenotype. J. Biol. Chem. *285*, 6153–6160.

51. Emanuelli, B., Vienberg, S.G., Smyth, G., Cheng, C., Stanford, K.I., Arumugam, M., Michael, M.D., Adams, A.C., Kharitonenkov, A., and Kahn, C.R. (2014). Interplay between FGF21 and insulin action in the liver regulates metabolism. J. Clin. Invest. *124*, 515–527.

52. Samms, R.J., Smith, D.P., Cheng, C.C., Antonellis, P.P., Perfield, J.W., 2nd, Kharitonenkov, A., Gimeno, R.E., and Adams, A.C. (2015). Discrete aspects of FGF21 in vivo pharmacology do not require UCP1. Cell Rep. *11*, 991–999.

53. Wang, Y., Rimm, E.B., Stampfer, M.J., Willett, W.C., and Hu, F.B. (2005). Comparison of abdominal adiposity and overall obesity in predicting risk of type 2 diabetes among men. Am. J. Clin. Nutr. *81*, 555–563.

54. Carey, V.J., Walters, E.E., Colditz, G.A., Solomon, C.G., Willett, W.C., Rosner, B.A., Speizer, F.E., and Manson, J.E. (1997). Body fat distribution and risk of non-insulin-dependent diabetes mellitus in women. The Nurses' Health Study. Am. J. Epidemiol. *145*, 614–619.

55. Misra, A., Garg, A., Abate, N., Peshock, R.M., Stray-Gundersen, J., and Grundy, S.M. (1997). Relationship of anterior and posterior subcutaneous abdominal fat to insulin sensitivity in nondiabetic men. Obes. Res. *5*, 93–99.

56. Murray, S.A., Dalbøge, L.S., Baquero, K., Sanford, C.A., Misquith, A., Mercer, A.J., Meek, T.H., Guldbrandt, M., Andersen, B., Kievit, P., et al. (2020). Whole transcriptome analysis and validation of metabolic pathways in subcutaneous adipose tissues during FGF21-induced weight loss in non-human primates. Sci. Rep. *10*, 7287.

57. Zuriaga, M.A., Fuster, J.J., Gokce, N., and Walsh, K. (2017). Humans and Mice Display Opposing Patterns of "Browning" Gene Expression in Visceral and Subcutaneous White Adipose Tissue Depots. Front. Cardiovasc. Med *4*, 27.

58. Dewal, R.S., and Stanford, K.I. (2019). Effects of exercise on brown and beige adipocytes. Biochim. Biophys. Acta Mol. Cell Biol. Lipids *1864*, 71–78.

59. Chusyd, D.E., Wang, D., Huffman, D.M., and Nagy, T.R. (2016). Relationships between Rodent White Adipose Fat Pads and Human White Adipose Fat Depots. Front. Nutr. *3*, 10.

60. Zilkha, N., Kuperman, Y., and Kimchi, T. (2017). High-fat diet exacerbates cognitive rigidity and social deficiency in the BTBR mouse model of autism. Neuroscience *345*, 142–154.

61. Heo, Y., Zhang, Y., Gao, D., Miller, V.M., and Lawrence, D.A. (2011). Aberrant immune responses in a mouse with behavioral disorders. PLoS ONE *6*, e20912.

62. Degirolamo, C., Sabbà, C., and Moschetta, A. (2016). Therapeutic potential of the endocrine fibroblast growth factors FGF19, FGF21 and FGF23. Nat. Rev. Drug Discov. *15*, 51–69.

63. Frasca, D., Blomberg, B.B., and Paganelli, R. (2017). Aging, Obesity, and Inflammatory Age-Related Diseases. Front. Immunol. *8*, 1745.

64. Sponton, C.H., and Kajimura, S. (2018). AAV-mediated gene therapy as a strategy to fight obesity and metabolic diseases. EMBO Mol. Med. *10*, e9431.

65. Alexander, I.E., Cunningham, S.C., Logan, G.J., and Christodoulou, J. (2008). Potential of AAV vectors in the treatment of metabolic disease. Gene Ther. *15*, 831–839.

66. Lee, M.-J., Wu, Y., and Fried, S.K. (2013). Adipose tissue heterogeneity: implication of depot differences in adipose tissue for obesity complications. Mol. Aspects Med. *34*, 1–11.

67. Genkinger, J.M., Kitahara, C.M., Bernstein, L., Berrington de Gonzalez, A., Brotzman, M., Elena, J.W., Giles, G.G., Hartge, P., Singh, P.N., Stolzenberg-Solomon, R.Z., et al. (2015). Central adiposity, obesity during early adulthood, and pancreatic cancer mortality in a pooled analysis of cohort studies. Ann. Oncol. *26*, 2257–2266.

68. Hidayat, K., Yang, C.-M., and Shi, B.-M. (2018). Body fatness at an early age and risk of colorectal cancer. Int. J. Cancer *142*, 729–740.

69. García-Jiménez, C., Gutiérrez-Salmerón, M., Chocarro-Calvo, A., García-Martinez, J.M., Castaño, A., and De la Vieja, A. (2016). From obesity to diabetes and cancer: epidemiological links and role of therapies. Br. J. Cancer *114*, 716–722.

70. Pearson-Stuttard, J., Zhou, B., Kontis, V., Bentham, J., Gunter, M.J., and Ezzati, M. (2018). Worldwide burden of cancer attributable to diabetes and high body-mass index: a comparative risk assessment. Lancet Diabetes Endocrinol. *6*, e6–e15.

71. Mao, R., Kurada, S., Gordon, I.O., Baker, M.E., Gandhi, N., McDonald, C., Coffey, J.C., and Rieder, F. (2019). The mesenteric fat and intestinal muscle interface: creeping fat influencing stricture formation in Crohn's disease. Inflamm. Bowel Dis. *25*, 421–426.

72. Kahn, C.R., Wang, G., and Lee, K.Y. (2019). Altered adipose tissue and adipocyte function in the pathogenesis of metabolic syndrome. J. Clin. Invest. *129*, 3990–4000.

73. Scheja, L., and Heeren, J. (2019). The endocrine function of adipose tissues in health and cardiometabolic disease. Nat. Rev. Endocrinol. *15*, 507–524.

74. Colella, P., Ronzitti, G., and Mingozzi, F. (2017). Emerging Issues in AAV-Mediated *In Vivo* Gene Therapy. Mol. Ther. Methods Clin. Dev. *8*, 87–104.

75. Bates, R., Huang, W., and Cao, L. (2020). Adipose Tissue: An Emerging Target for Adeno-associated Viral Vectors. Mol. Ther. Methods Clin. Dev. *19*, 236–249.

76. Li, C., and Samulski, R.J. (2020). Engineering adeno-associated virus vectors for gene therapy. Nat. Rev. Genet. *21*, 255–272.

77. Charbel Issa, P., De Silva, S.R., Lipinski, D.M., Singh, M.S., Mouravlev, A., You, Q., Barnard, A.R., Hankins, M.W., During, M.J., and Maclaren, R.E. (2013). Assessment of tropism and effectiveness of new primate-derived hybrid recombinant AAV serotypes in the mouse and primate retina. PLoS ONE *8*, e60361.

78. Huang, W., Queen, N.J., and Cao, L. (2019). rAAV-Mediated Gene Delivery to Adipose Tissue. Methods Mol. Biol. *1950*, 389–405.

79. Bagchi, D.P., and MacDougald, O.A. (2019). Identification and Dissection of Diverse Mouse Adipose Depots. J. Vis. Exp. *2019*, https://doi.org/10.3791/59499.

80. Folch, J., Lees, M., and Sloane Stanley, G.H. (1957). A simple method for the isolation and purification of total lipides from animal tissues. J. Biol. Chem. *226*, 497–509.

81. Livak, K.J., and Schmittgen, T.D. (2001). Analysis of relative gene expression data using real-time quantitative PCR and the 2(-Delta Delta C(T)) Method. Methods *25*, 402–408.

82. Fraulob, J.C., Ogg-Diamantino, R., Fernandes-Santos, C., Aguila, M.B., and Mandarim-de-Lacerda, C.A. (2010). A Mouse Model of Metabolic Syndrome: Insulin Resistance, Fatty Liver and Non-Alcoholic Fatty Pancreas Disease (NAFPD) in C57BL/6 Mice Fed a High Fat Diet. J. Clin. Biochem. Nutr. *46*, 212–223.